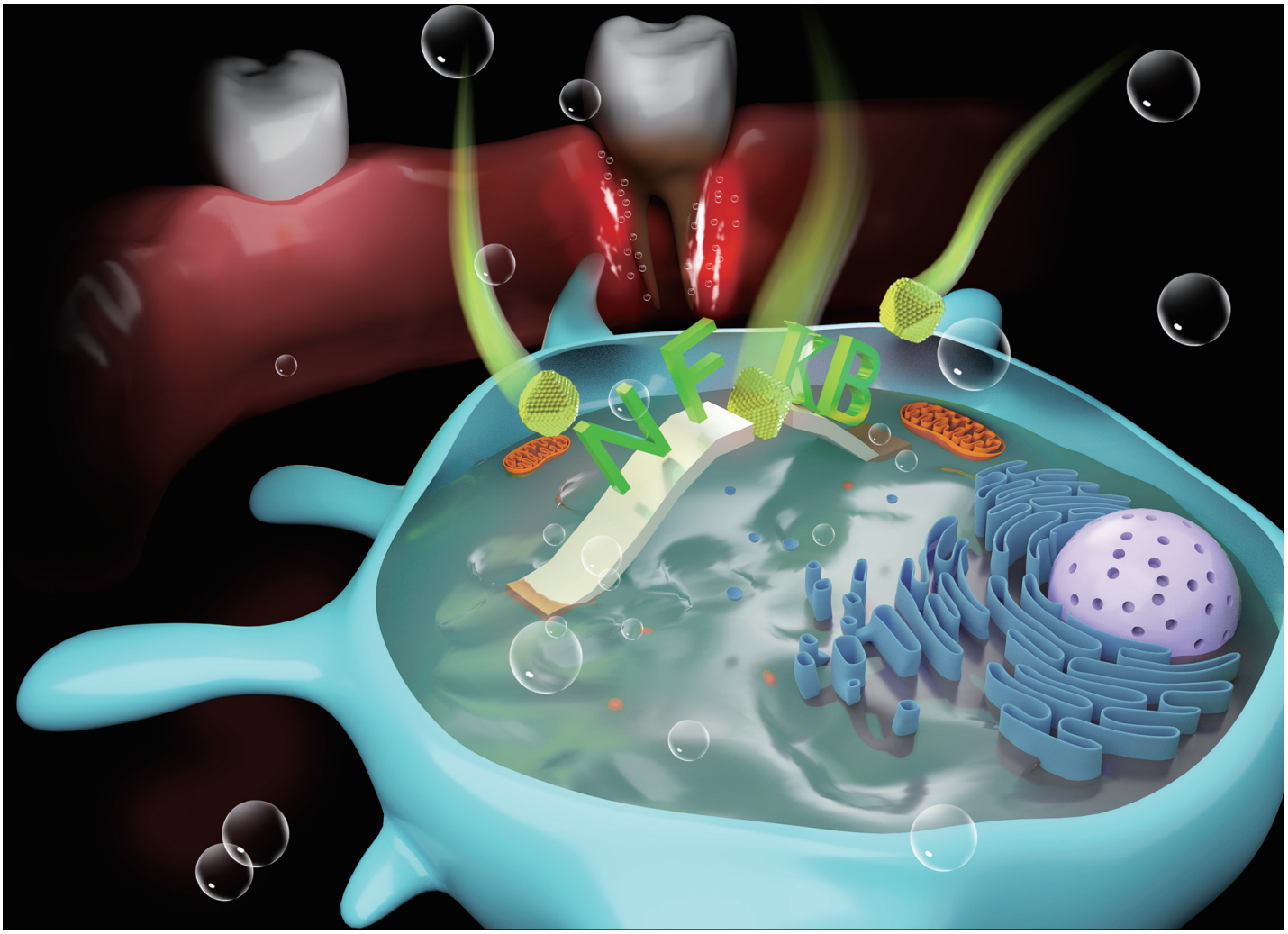

Showcasing research from Prof. Leiying Miao's group at Jiangsu Provincial Key Medical Discipline Center Lab, Nanjing Stomatology Hospital, Medical School of Nanjing University, Nanjing, China.

Cerium oxide nanozyme attenuates periodontal bone destruction by inhibiting the ROS–NFκB pathway

A multi-enzyme mimicking cerium oxide (CeO_2) nanozyme has been synthesized. The comet-like CeO_2 nanozyme eliminates reactive oxygen species (ROS) around the periodontal microenvironment and plays a part in anti-inflammation through inhibiting the NFκB signaling pathway. From the results of a rat periodontitis model, CeO_2 appears to possess great promise in the clinical management of periodontitis.

As featured in:

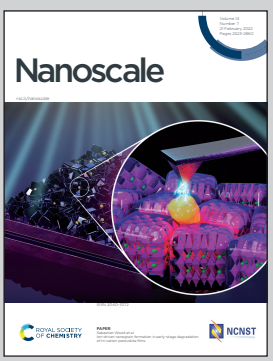

See Jiangjiexing Wu, Hui Wei, Leiying Miao *et al.*, *Nanoscale*, 2022, **14**, 2628.

ROYAL SOCIETY OF CHEMISTRY

rsc.li/nanoscale

Registered charity number: 207890

Nanoscale

PAPER

View Article Online
View Journal | View Issue

Cite this: *Nanoscale*, 2022, **14**, 2628

Cerium oxide nanozyme attenuates periodontal bone destruction by inhibiting the ROS–NFκB pathway†

Yijun Yu,‡[a] Sheng Zhao,‡[b] Deao Gu,[c] Bijun Zhu,[a] Hanxiao Liu,[a] Wenlei Wu,[d] Jiangjiexing Wu, *[b,e] Hui Wei *[b] and Leiying Miao*[a]

Periodontitis, an inflammatory disease of oxidative stress, occurs due to excess reactive oxygen species (ROS) contributing to cell and tissue damage which in turn leads to alveolar bone resorption as well as the destruction of other periodontal support tissues. With significant recent advances in nanomaterials, we considered a unique type of nanomaterials possessing enzyme-like characteristics (called nanozymes) for potential future clinical applications, especially in light of the increasing number of studies evaluating nanozymes in the setting of inflammatory diseases. Here, we introduced a therapeutic approach for the management of periodontitis utilizing an injection of cerium oxide nanoparticles (CeO_2 NPs) *in situ*. In this study, our synthesized CeO_2 NPs could act as ROS scavengers in the inflammatory microenvironment with ideal outcomes. *In vitro* and *in vivo* experiments provide strong evidence on the roles of CeO_2 NPs in scavenging multiple ROS and suppressing ROS-induced inflammation reactions stimulated by lipopolysaccharides. Moreover, CeO_2 NPs could inhibit the MAPK–NFκB signalling pathway to suppress inflammatory factors. In addition, the results from a rat periodontitis model demonstrate that CeO_2 NPs could exhibit a remarkable capacity to attenuate alveolar bone resorption, decrease the osteoclast activity and inflammation, and consequently improve the restoration of destroyed tissues. Collectively, our present study underscores the potential of CeO_2 NPs for application in the treatment of periodontitis, and provides valuable insights into the application of nanozymes in inflammatory diseases.

Received 14th September 2021,
Accepted 7th January 2022

DOI: 10.1039/d1nr06043k

rsc.li/nanoscale

Introduction

Periodontitis is a common disease which is characterized by the destruction of tooth-supporting tissues, including alveolar bone, cementum, and periodontal ligament.[1] The pathogenesis of periodontitis involves the interplay of periodontal pathogens and the host immune response.[2,3] Polymorphonuclear neutrophils play an essential role in the maintenance of periodontal health and act as the first line of defence in the innate immune system. Interestingly, "hyperactivated" polymorphonuclear neutrophils, characterized by the overproduction of reactive oxygen species (ROS), appear to be associated with periodontal diseases.[4] ROS include hydrogen peroxide (H_2O_2), superoxide ($O_2^{\bullet-}$), hydroxyl radical ($^{\bullet}OH$), and singlet oxygen ($^1O_2$).[5] Importantly, ROS can be considered as a double-edged sword, as they help destroy pathogens to keep health,[6] while contribute to oxidative stress when their levels are excessive.[7] Although ROS play an important role in cell signalling, an excess of ROS results in direct cell and tissue damage including lipid peroxidation, protein oxidation, and mitochondrial depolarization.[8] Furthermore, ROS activate NFκB signalling and thereby promotes inflammation.[9] Interestingly, ROS-mediated intracellular signalling induces osteoclastogenesis and this eventually results in bone tissue damage around teeth.[10] Data from a systematic review revealed plasma, serum and salivary total antioxidant concentrations to

[a]*Department of Cariology and Endodontics, Nanjing Stomatological Hospital, Medical School of Nanjing University, Nanjing, Jiangsu 210008, China. E-mail: miaoleiying80@163.com*
[b]*Department of Biomedical Engineering, College of Engineering and Applied Sciences, Nanjing National Laboratory of Microstructures, Jiangsu Key Laboratory of Artificial Functional Materials, Chemistry and Biomedicine Innovation Center (ChemBIC), Nanjing University, Nanjing, Jiangsu 210023, China. E-mail: weihui@nju.edu.cn*
[c]*Department of Orthodontics, Nanjing Stomatological Hospital, Medical School of Nanjing University, Nanjing, Jiangsu 210008, China*
[d]*Nanjing Stomatological Hospital, Medical School of Nanjing University, Nanjing, Jiangsu 210008, China*
[e]*School of Marine Science and Technology, Tianjin University, Tianjin 300072, China. E-mail: wujiangjiexing2007@126.com*
†Electronic supplementary information (ESI) available. See DOI: 10.1039/d1nr06043k
‡These authors contributed to this work equally.

be decreased in periodontitis patients as compared with healthy controls.[11] Taken into consideration the detrimental effects exerted by excess ROS levels, a therapeutic strategy targeted to scavenge ROS and thus alleviate inflammation could be an effective therapeutic approach for the management of periodontitis. Many studies investigating treatments for periodontitis are typically performed with natural antioxidants such as resveratrol,[12] paeonol,[13] and coenzyme Q10,[14] which react with ROS stoichiometrically and therefore are consumable. Thus, more efficient therapies targeting ROS need to be further developed.

An increasing number of functionalized nanomaterials have been discovered to play biomedical roles due to certain inherent properties such as photothermal,[15] superparamagnetic,[16] and fluorescence effects.[17] Among them, an emerging field of nanomaterials termed as "nanozymes" has been opened since 2007, which were defined as nanomaterials possessing enzyme-like characteristics.[18–26] Increasing reports have investigated nanozymes with ROS-scavenging properties that can potentially be used for treating a wide variety of inflammatory diseases including Alzheimer's disease,[27–29] rheumatoid arthritis,[30,31] and inflammatory bowel disease.[32,33] It is worth mentioning that cerium oxide nanoparticles (CeO_2 NPs), a typical and widely-explored nanozyme, have been found to possess activities that mimic those of a number of enzymes, including superoxide dismutase (SOD) and catalase (CAT) like-activity, and oxidase-mimicking activity[34] as well as $^{\bullet}OH$ scavenging properties due to the presence of mixed valence states (Ce^{3+} and Ce^{4+}).[35–41] Increasingly, studies have focused on elucidating mechanisms responsible for the SOD- and CAT-like properties of nanoceria, based in particular on Gao's work at the atomic level.[42,43] The enzyme-mimicking activities of CeO_2 NPs could be modulated by changing the crystal environment.[44] Until now, CeO_2 NPs have been evaluated for their potency in the setting of various inflammatory diseases including neurodegenerative illnesses,[27,28] acute kidney injury,[35,45] ocular surface disease,[46] *etc*. For example, vacancy-engineered CeO_2 NPs have been reported to prevent increases in intracellular reactive oxygen intermediates in rat retinal cells, and *in vivo*, also prevented the loss of vision.[35] In another work,[45] CeO_2 modified with triphenylphosphine was used in the treatment of acute kidney injury, showing promising *in vitro* and *in vivo* outcomes. Our previous work involved the design of a nanozyme with a formulation of CeO_2@MMT for oral administration, and was found to effectively control inflammatory bowel disease.[32] Based on prior work on CeO_2, we put forward a hypothesis that CeO_2 NPs could greatly decrease the excessive levels of ROS in the periodontal microenvironment, and thus be eutherapeutic for periodontitis. Although exploration of the therapeutic effect of CeO_2 NPs in the setting of various types of diseases is drawing increasing attention, few studies have, to date, delved into the elucidation of the anti-inflammatory mechanism of CeO_2.

To demonstrate our hypothesis, as shown in Scheme 1, CeO_2 NPs were synthesized as in our previous work[32] and their effect on periodontitis was investigated. First, CeO_2 NPs were confirmed to possess SOD- and CAT-like activities, as well as $^{\bullet}OH$ scavenging ability. Thus, CeO_2 NPs were defined as possessing nanozyme characteristics. Both the *in vitro* and *in vivo* results revealed that CeO_2 decreased the excess ROS generated by the presence of lipopolysaccharides (LPS). Moreover, the mechanistic study revealed that CeO_2 decreased inflammation *via* inhibition of the MAPK–NFκB signalling pathway. Finally, CeO_2 was found to attenuate periodontal destruction induced by ligation in rats. These findings collectively lay a foundation for future clinical application of nanozymes in the treatment of periodontitis.

Jiangjiexing Wu

Jiangjiexing Wu is an Associate Professor at Tianjin University. She received her B.S. degree and Ph.D. degree from Tianjin University (advisor: Professors Wei Li and Yi Lu). As a joint Ph.D. student, she also studied in Professor Yi Lu's group at the University of Illinois at Urbana-Champaign for two years. After graduation, she joined Professor Hui Wei's group at Nanjing University as a Research Associate Professor before she moved to Tianjin University. Her research interests focus on the rational design and synthesis of functional nanomaterials (such as nanozymes) for analytical, biomedical, and environmental applications.

Experimental

Detection of multi-enzyme mimicking activities of CeO_2 NPs

The SOD-mimicking activity of CeO_2 NPs was detected using a SOD assay kit (Dojindo). The reaction between WST-1 and $O_2^{\bullet-}$ produced a water-soluble coloured product which could be detected using a microplate reader. While SOD inhibited the reduction reaction of $O_2^{\bullet-}$ by WST-1, SOD-mimicking activity could be calculated from the absorbance values of different groups.

The hydroxyl radical scavenging activity of CeO_2 NPs was investigated using a hydroxyl radical assay kit (Nanjing Jiancheng Bioengineering Institute). The Griess reagent reacted with $^{\bullet}OH$ generated from the Fenton reaction of Fe^{2+} and H_2O_2; the absorbance value at 550 nm thus reflected the quantity of $^{\bullet}OH$ present. Elimination of $^{\bullet}OH$ was calculated utilizing the following equation: elimination ability (U mL^{-1}) = $(A_c - A_x)/(A_s - A_0) \times 8.824$ mmol L^{-1}; where A_c denotes the control absorbance value, A_x denotes the absorbance value of CeO_2 solutions at different concentrations, A_s denotes the standard absorbance value, and A_0 denotes the blank absorbance value.

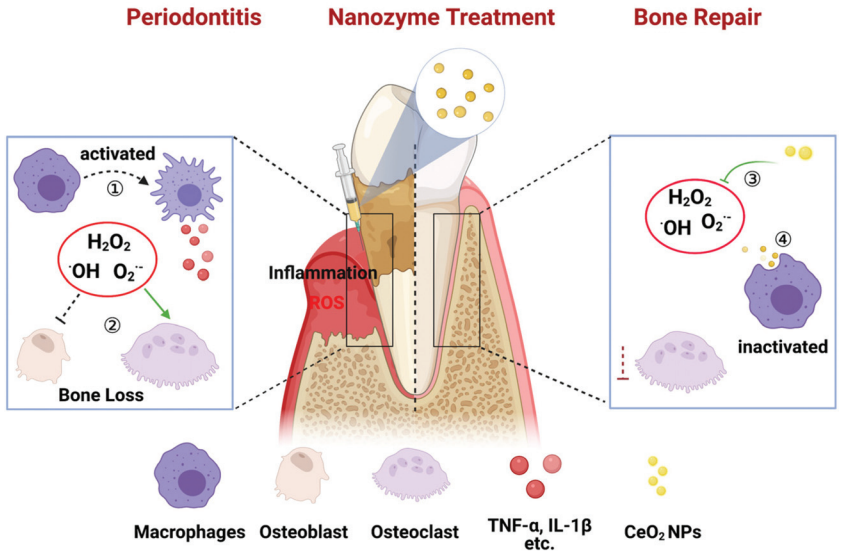

Scheme 1 Schematic illustration of the effect of CeO_2 NPs on periodontitis treatment. In the periodontitis microenvironment, ROS induced the activation of macrophages, leading to the release of pro-inflammatory cytokines such as TNF-α, IL-1β and so on. ROS inhibited the survival and differentiation of osteoblasts, while promoted the activity of osteoclast, and consequently resulted in the bone loss. With the treatment of CeO_2 NPs, ROS was scavenged by CeO_2 NPs, and inflammation could be restrained by the inhibition of the NFκB signalling pathway in macrophages. Therefore, there would appear bone repair in periodontal destruction.

Since CAT decomposes H_2O_2 into H_2O and O_2, the amount of O_2 generated indirectly reflected the capacity of CeO_2 NPs to decompose H_2O_2. Absorbance at 405 nm was detected after reaction with dopamine and the $\Delta OD_{405\ nm}$ value was calculated to represent CAT-mimicking activity.

Intracellular ROS scavenging activity of CeO_2 NPs

To investigate the ROS scavenging activity of CeO_2 NPs, the cells were co-cultured with CeO_2 NPs for 4 h and stimulated with LPS for 12 h, then washed twice with PBS and incubated with a 10 μM DCFH-DA probe for 5–10 min. Importantly, the cells were washed with HEPES buffered Krebs-Ringer solution after probe loading and before observation under a confocal microscope.

In vitro anti-inflammatory and anti-oxidative studies

RAW 264.7 cells were seeded into 6-well plates at a density of 1×10^5 per well for RNA and protein extraction. CeO_2 NPs at varying concentrations were added and co-cultured with the cells for 4 h, and LPS (20 ng mL^{-1}) was subsequently added into the media for another 3 h for mRNA analysis and 18 h for protein level detection. Detailed steps and procedures of real-time PCR and western blot are provided in the ESI.†

To investigate the possible anti-inflammatory activity, CeO_2 NPs were added and co-cultured with cells for 4 h at different concentrations. Then, LPS (20 ng mL^{-1}) was added into the medium for another 30 min. The extraction process of total protein was as previously described, apart from RIPA supplementation with a phosphatase inhibitor cocktail (ThermoFisher Scientific). The p-p65, p65, and IκBα primary antibodies were purchased from Affinity Biosciences; the dilution ratio was 1 : 500. The other primary antibodies of MAPK (p-p38, p-38, p-ERK1/2, ERK1/2, p-JNK and JNK) were purchased from Cell Signalling Technology and used with a dilution ratio of 1 : 1000. Western blotting was performed to evaluate the expression of the key molecules of NFκB and MAPK.

Immunofluorescence detection of p65 nuclear translocation

To evaluate the nuclear translocation of NF-κB/p65, RAW 264.7 cells were pretreated with or without CeO_2 NPs for 4 h and stimulated with LPS for 30 min. The cells were then fixed with 4% paraformaldehyde and permeabilized with 0.5% Triton-100 for 20 min. After blocking with 1% skim milk for 30 min, the cells were incubated with the p65 antibody (Affinity Biosciences, 1 : 400) for 2 h at room temperature and then with the Alexa Fluor 488-conjugated secondary antibody (1 : 400) for 1 h at room temperature. Finally, the cells were stained with DAPI (visualized in blue) for observation under a confocal microscope.

Establishment of a rat ligation-induced periodontitis model

All animal experiments were approved by the Animal Ethics Committee of Nanjing University and carried out in accordance with the National Institutes of Health Guide for the Care and Use of Laboratory Animals.

Six-week-old male Sprague Dawley rats were acclimatized a week before modelling. Experimental time points are listed in Fig. S13.† All rats were randomly divided into control (normal untreated rats, n = 8), sham (ligation immediately removed postoperatively, n = 8), ligature (rats with ligation-induced periodontitis, n = 8), and Lig + CeO_2 (rats treated with CeO_2 NPs,

n = 8) groups. Briefly, the rats were anesthetized with chloral hydrate (7%; 0.4 mL per 100 g) *via* peritoneal injection. The rats were fixed in the supine position and a 0.2 mm ligature wire was inserted through the interproximal space around the maxillary second molar and fixed on the buccal side. One week after this procedure, CeO_2 NPs (10 μL; 2 mg mL^{-1}) were injected into the central of palatal gingiva of the maxillary second molar every 3 d. The appointed time was 1 week and 4 weeks from the first injection of CeO_2 NPs. All rats were sacrificed by anesthetic overdose. The maxillary bone and viscera were fixed in 10% neutral buffered formalin before observation.

Micro-CT analysis

Samples were scanned with a micro-CT system at a source voltage of 65 kV, a source current of 385 μA, and a scanning thickness of 18 μm. A three-dimensional reconstruction was subsequently performed. The distance from the cemento-enamel junction (CEJ) to the alveolar bone crest (ABC) was measured at 6 sites, including the mesial, middle, and distal palatal, and buccal regions, to represent the loss of attachment and destruction of periodontal bone tissues.

Histological evaluation

Maxillary tissues were decalcified, dehydrated, and cut into slices for histological observation. Haematoxylin-eosin (H&E) and Masson trichrome stainings were used to evaluate the general changes in periodontal tissues. Tartrate resistant acid phosphatase (TRAP) staining was performed to specifically mark osteoclastic activity, while iNOS and NFκB expressions around the maxillary second molar were measured by immunohistochemistry. The histopathology sections of vital viscera including the heart, liver, spleen, lungs, and kidneys were used to evaluate the CeO_2 NP toxicity. All slices were scanned using a 3D HISTECH slice scanner and analysed with the CaseViewer software.

Statistical analysis

Statistical analyses were performed with Graphpad Prism 8 using the one-way analysis of variance. Numerical data are expressed as the mean ± SD and $P < 0.05$ was considered to be statistically significant.

Results and discussion

Characterization of the enzyme-mimicking activity of CeO_2 NPs

CeO_2 NPs were synthesized as shown in Fig. 1a. TEM revealed that the CeO_2 NPs were spherical and had a size of approximately 5 nm and uniformly dispersed without apparent agglomeration (Fig. 1b). High-resolution TEM imaging revealed well-resolved lattice planes spaced at approximately 0.31 nm between adjacent lattices (inset in Fig. 1b). Dynamic light scattering revealed the hydrate particle size to be approximately 10 nm (Fig. S1†). In addition, the ζ potential of CeO_2 NPs was measured to be approximately −30.13 mV. XRD was employed to analyse the phase composition and crystallinity of the NPs. As seen in the diffraction pattern shown in Fig. 1c, the peaks at 28.61°, 47.59° and 56.48° coincided with the characteristic peaks of CeO_2 crystals and corresponded to the (111), (220), and (311) lattice planes, respectively. XPS revealed the valences of Ce^{3+} and Ce^{4+} among the NPs (Fig. S2†). Thus, the successful synthesis of CeO_2 NPs was confirmed.

$O_2^{\bullet-}$, one common type of ROS, is eliminated by natural SOD.[47] To investigate the SOD-mimicking activity of CeO_2 NPs, different concentrations of NPs were evaluated using a SOD Assay Kit. The results revealed the SOD-like catalytic activity of CeO_2 NPs to be dose-dependent, with the $O_2^{\bullet-}$ elimination per-

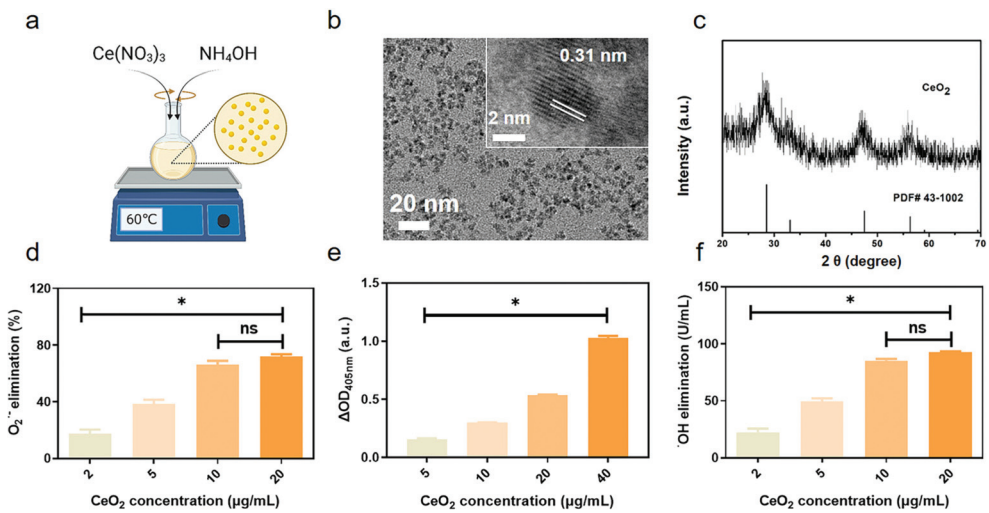

Fig. 1 The characterization analysis and enzyme-mimicking activities of CeO_2 NPs. (a) Synthesis scheme of CeO_2; (b) TEM images; (c) XRD spectrum; (d) SOD-like activity of CeO_2 NPs at different concentrations; (e) CAT-like activity; and (f) $^{\bullet}OH$ elimination ability. ns means $P > 0.05$ and * means $P < 0.05$.

centage reaching nearly 70% at a concentration of 20 μg mL^{-1} (Fig. 1d). In living organisms, hydrogen peroxide is generated when $O_2^{\bullet-}$ is eliminated by SOD. In addition, H_2O_2 is another kind of destructive ROS that can persist for significant periods of time.[48] The ability of CeO_2 NPs to decompose H_2O_2 was also studied. As shown in Fig. 1e, the CAT-mimicking activity of CeO_2 NPs was concentration dependent. $^{\bullet}OH$ can be generated from H_2O_2 *via* the Fenton reaction; its strong oxidizing properties damage cell viability and no natural enzyme can effectively scavenge $^{\bullet}OH$.[49] To determine the $^{\bullet}OH$ scavenging ability of CeO_2 NPs, different concentrations of CeO_2 NPs were added into a reaction mixture. The elimination of $^{\bullet}OH$ was detected by the absorption values of the reaction mixture. As shown in Fig. 1f, $^{\bullet}OH$ elimination increased as the concentration of CeO_2 NPs increased, reaching 80 U mL^{-1} at a concentration of 20 μg mL^{-1}. We thus concluded that CeO_2 NPs exhibited excellent SOD- and CAT-like activities. Moreover, they were highly efficient in eliminating $^{\bullet}OH$. These findings were in accordance with other researches[43] and underscore how CeO_2 NPs may be used as nanozymes in the future.

CeO_2 NPs reduce intracellular ROS levels in the setting of LPS stimulation

To detect whether CeO_2 NPs could reduce intracellular ROS levels, RAW 264.7 cells stimulated with LPS were used to establish a model of inflammation. No obvious cytotoxicity of CeO_2 NPs at concentrations up to 1000 μg mL^{-1} was detected by the CCK-8 assay (Fig. S3†). Findings also confirmed that the intracellular levels of ROS were elevated after stimulation by 20 and 100 ng mL^{-1} of LPS for 12 h (Fig. S4a†). Meanwhile, the cells treated with 20 ng mL^{-1} of LPS for 12 h and 18 h exhibited enhanced green ROS fluorescence. Consequently, stimulation using 20 ng mL^{-1} of LPS for 12 h was considered to be sufficient for ROS generation. As shown in Fig. 2, a markedly elevated fluorescence intensity was detected in the LPS-treated group, indicating that the ROS levels appeared to increase when stimulated with LPS for 12 h. Moreover, changes in the cellular morphology from round into spindle-like shapes with greater numbers of pseudopodia were noted in comparison with controls, which exhibited round shapes. Green fluorescence on imaging as well as quantitative intensities indicated that the ROS levels dramatically decreased in cells which were pre-incubated with CeO_2 NPs. In addition, the ROS levels of the control and CeO_2 NP-treated groups were not significantly different.

CeO_2 NPs possess anti-inflammatory and anti-oxidant activity in RAW 264.7 cells

Encouraged by the above results, we further evaluated the anti-inflammatory and anti-oxidant activities of CeO_2 NPs. A 20 ng mL^{-1} content of LPS was selected according to real-time PCR (Fig. S5†) and western blot (Fig. S6†) data as 20 ng mL^{-1} of LPS was found to up-regulate IL-1β and TNF-α mRNA levels approximately 2000 and 40 times, respectively, as well as increase the protein expression of iNOS. In subsequent experiments, CeO_2 NPs were incubated with the cells before LPS stimulation. As shown in Fig. 3, the IL-1β mRNA levels were down-regulated from 4000 to 1000 times as the concentration of CeO_2 NPs increased. A similar trend was also observed with TNF-α. A significant difference between the LPS and CeO_2 NPs groups was also noted. The levels of iNOS mRNA expression were found to decrease due to effects exerted by the CeO_2 NPs. The levels of iNOS protein expression (Fig. 3d) similarly decreased in a concentration-dependent manner.

The Nrf2–ARE pathway, an important anti-oxidant regulatory mechanism, balances the oxidation and anti-oxidation

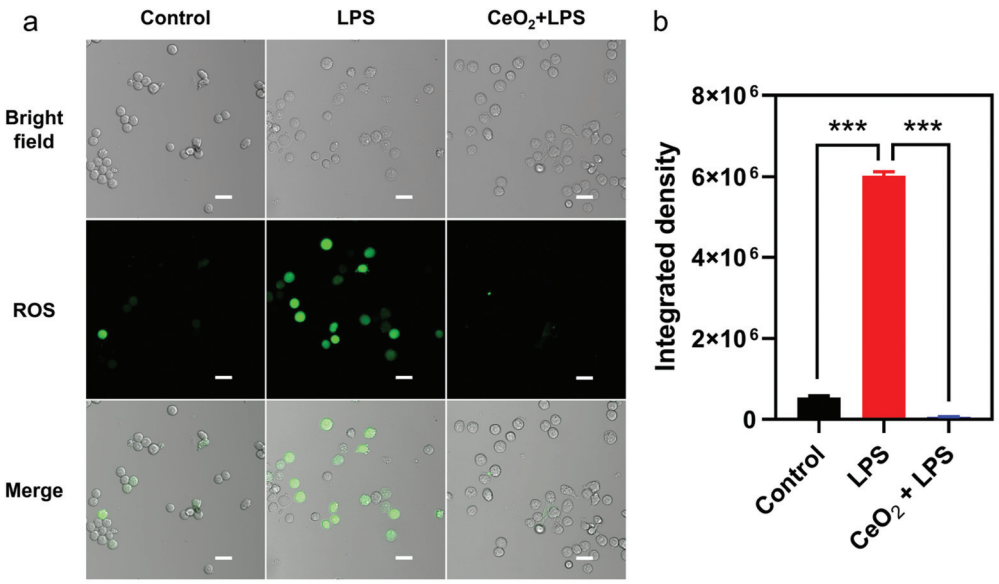

Fig. 2 The intracellular ROS levels in RAW 264.7 cells treated with LPS alone and the combined application of 20 μg mL^{-1} CeO_2 NPs. (a) The intracellular ROS level induced by LPS for 12 h and (b) the semiquantitative analysis of a. Scale bar: 20 μm. *** means $P < 0.001$.

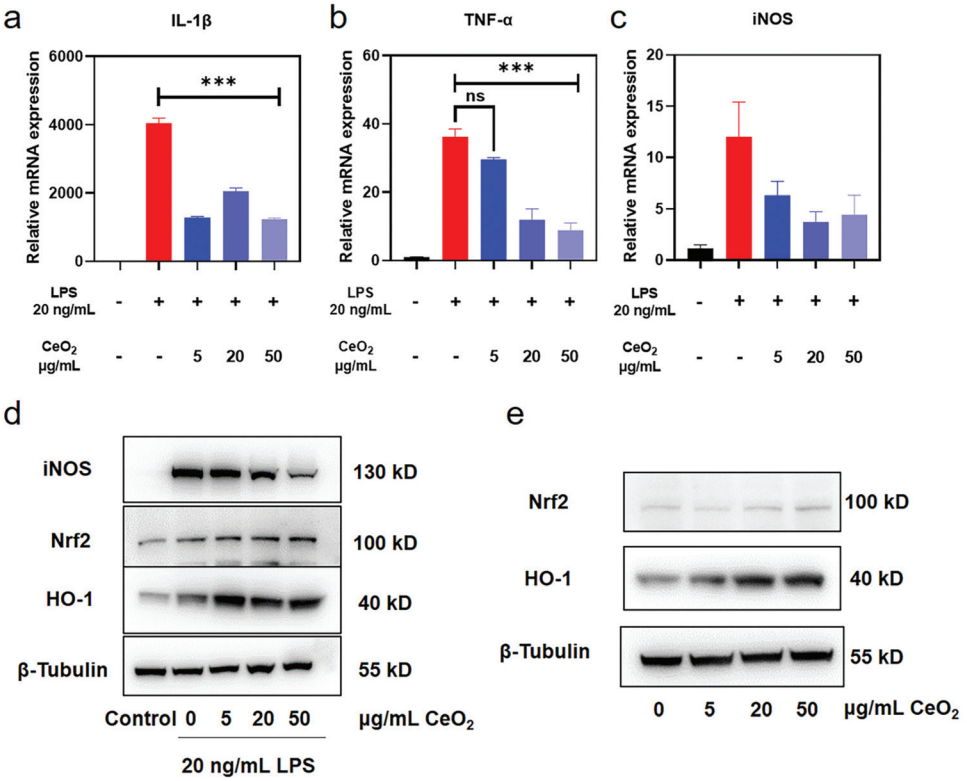

Fig. 3 The anti-inflammatory and anti-oxidative effects of CeO_2 NPs. (a) The relative mRNA expression of IL-1β stimulated with LPS and pre-treated with CeO_2 NPs; (b) the relative mRNA expression of TNF-α; (c) the relative mRNA expression of iNOS; (d) the protein expression of the key representative factors of inflammation and anti-oxidation; and (e) the activation effect of CeO_2 NPs on the expression of anti-oxidative related proteins. The WB bands were cropped to clarify the lanes, and the raw data are provided in the ESI (Fig. S15 and S16†). ns means $P > 0.05$ and *** means $P < 0.001$.

activities in healthy cells.[50] Downstream proteins of Nrf2–ARE include hemeoxygenase-1 (HO-1), NADPH quinone dehydrogenase 1 (NQO1) and the glutamate–cysteine ligase catalytic and modifier subunits (Gclc&Gclm). Western blot findings revealed the expression of HO-1 was markedly increased in cells pre-incubated with CeO_2 NPs after LPS stimulation (Fig. 3d and Fig. S7†). The levels of Nrf2 and HO-1 proteins were detected by western blot to further investigate the effect of CeO_2 NPs on the Nrf2–ARE pathway. As compared with the control group, the expression of Nrf2 and HO-1 increased as the concentration of CeO_2 NPs increased (Fig. 3e and Fig. S8†). These findings indicate that CeO_2 NPs activated Nrf2–HO-1 signalling and promoted associated protein expression to a certain extent.

CeO_2 NPs inhibit the MAPK–NFκB signalling pathway

Several key proteins of the TLR4–NFκB classical inflammatory pathway were detected to evaluate the possible anti-inflammatory effects of CeO_2 NPs. Mitogen activated protein kinase (MAPK) and NFκB are the main regulators of inflammation.[51] An increased expression of p-p65 was observed while the deceased expression of the IκBα protein in RAW 264.7 cells stimulated with LPS for 30 min, thus highlighting the activation of the NFκB pathway (Fig. S9†). The expression of p-p65 decreased as the concentrations of CeO_2 NPs increased while the IκBα level increased in a CeO_2 NP concentration-dependent manner (Fig. 4a and Fig. S10†). Immunofluorescence revealed that p-p65 (labelled in green) translocated into the nucleus in the setting of LPS stimulation and that CeO_2 NPs inhibited this process (Fig. 4c). The NFκB pathway was thus found to be inhibited by CeO_2 NPs.

As the NFκB pathway is downstream from the MAPK signalling pathway, key MAPK proteins were detected. Stimulation with LPS increased the p-ERK1/2, p-p38 and p-JNK expressions, which gradually decreased as the CeO_2 NP concentration increased (Fig. 4b and Fig. S11†). Moreover, CeO_2 NPs at a concentration of 50 μg mL^{-1} were found to exert the strongest inhibitory effect on MAPK. A previous study found that CeO_2 NPs attenuated severe sepsis induced by LPS and inhibited MAP kinase–NFκB mediated signalling.[52]

Thus, RAW 264.7 cell stimulation with LPS was found to result in TLR4 activation and the high levels of intracellular ROS production. After the activation of the MAPK–NFκB pathway, pro-inflammatory factors such as IL-1β and TNF-α were markedly up-regulated, further leading to more severe tissue damage.[53] When CeO_2 NPs entered the cells, their ROS scavenging activity directly attenuated the high levels of ROS. At the same time, Nrf2–HO-1 activation and HO-1 expression

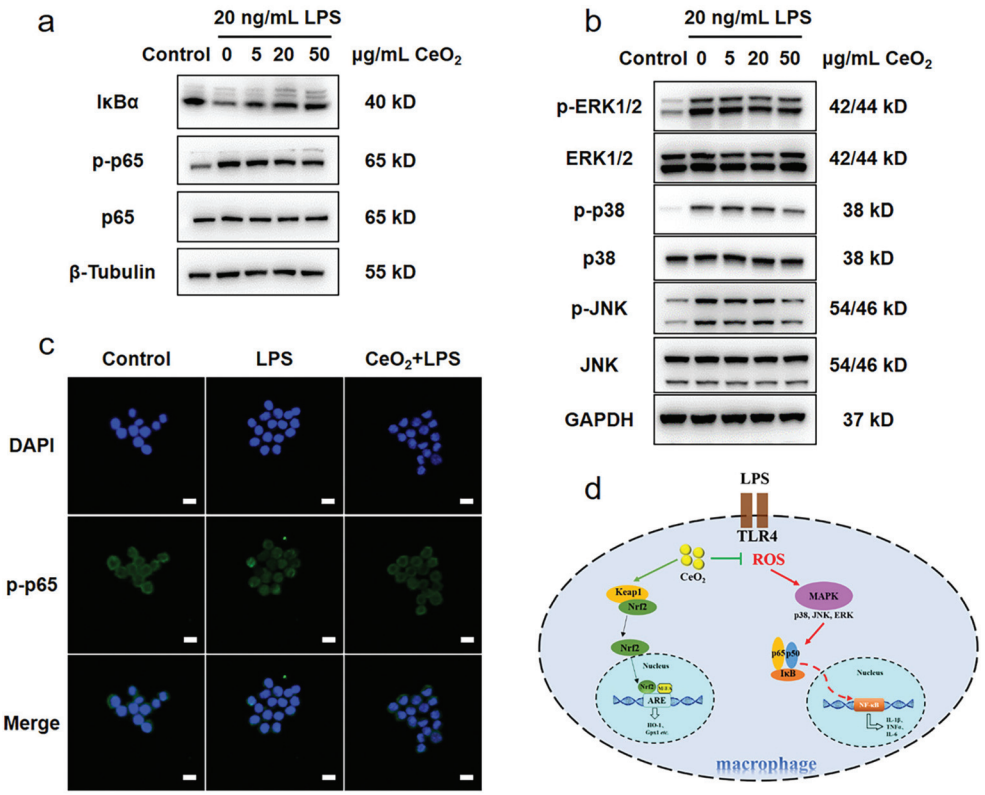

Fig. 4 The anti-inflammatory mechanism of CeO_2 NPs. (a) The effect of CeO_2 NPs on the protein expression of the key molecules of the NFκB signalling pathway and (b) the inhibition effect of CeO_2 NPs on the MAPK signalling pathway; the WB bands were cropped to clarify the lanes, and the raw data are provided in the ESI (Fig. S17 and S18†). (c) The nuclear translocation of p-p65, scale bar: 20 μm and (d) the schematic diagram of the anti-inflammatory mechanism of CeO_2 NPs.

provided powerful anti-oxidant support. The decrease in the ROS and pro-inflammatory cytokine levels was due to the inhibition of the MAPK–NFκB pathway (Fig. 4d).

CeO_2 NPs inhibit local gingival ROS production induced by LPS

A rat model of gingival inflammation as induced by LPS was used to investigate the ROS scavenging activity of CeO_2 NPs *in vivo*. As shown in Fig. S12,† significant fluorescence was noted in the anterior region of the mandible treated with LPS injection, reflecting elevated ROS levels due to LPS stimulation. Upon treatment with CeO_2 NPs, fluorescence in this region markedly decreased and the average fluorescence intensity decreased to less than 1×10^8 from 2.5×10^8 in the LPS group tissues. These data indicated that CeO_2 NPs could effectively scavenge ROS, the production of which resulted from LPS-induced inflammation. In a prior study of periodontal diseases, polydopamine NPs were investigated as ROS scavengers and were also found to suppress ROS-induced inflammation.[54] The relevant anti-inflammatory mechanism, however, was not detailed in that study.

CeO_2 NPs attenuate periodontal tissue destruction in a rat model of ligation periodontitis

Considering the significant anti-inflammatory and anti-oxidative effects of CeO_2 NPs, an *in vivo* study was performed to investigate whether such NPs could be applied in the management of periodontitis. Here, we devised a method to ligate the rat maxillary second molar and established a model of chronic periodontitis (Fig. S13†).

Based on the micro-CT data, bone loss was found to be marked after ligation procedures were performed around the maxillary second molars (Fig. 5). As time progressed, tissue destruction around the teeth in the ligature group was exacerbated and damage extended to the lower third of the root as compared with the control and sham groups. The statistical values of distances between the CEJ and the ABC from all six sites also revealed bone destruction. Injection of CeO_2 NPs into the tissues markedly mitigate bone destruction caused by ligation at both 1- and 4-week time points.

H&E staining revealed that the junctional epithelium in the control group rats remained attached to the CEJ, thus exhibiting no attachment loss (Fig. 6a and b). Moreover, the periodontal structure remained intact without any inflammatory infiltrate. The periodontal ligament fibers were well-organized and densely arranged, and there was no obvious damage noted in the sham group tissues. However, marked tissue destruction and a decrease in the attachment of junctional epithelium to the root were noted in the ligature group tissues, with recruitment of inflammatory cells to sites around the maxillary

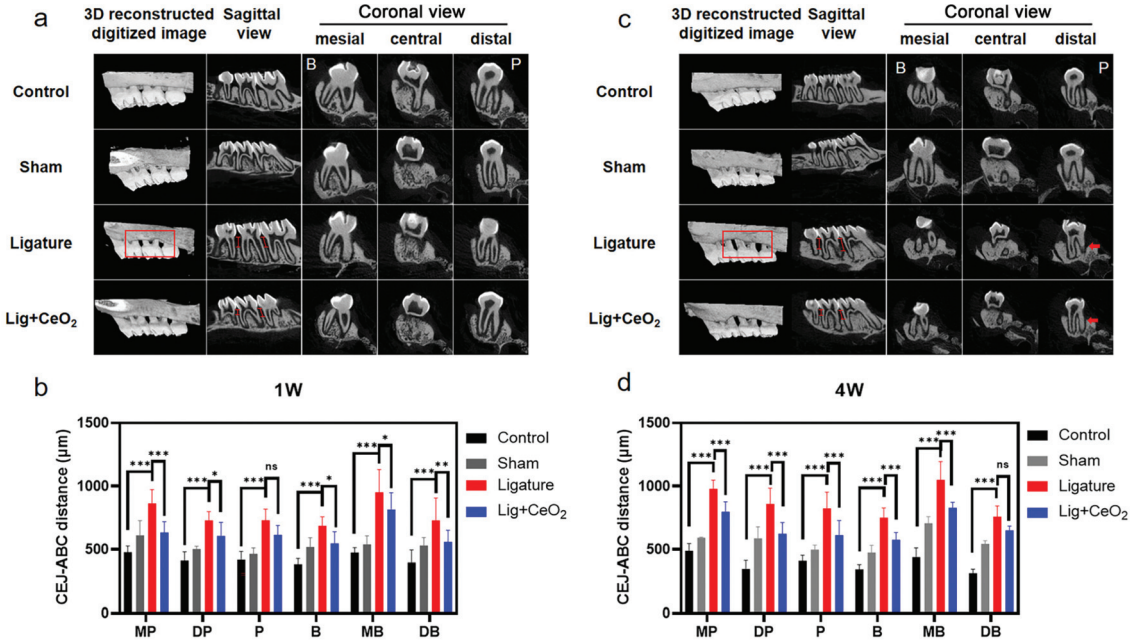

Fig. 5 The micro-CT analysis of a rat periodontitis model induced by ligature. (a) Different views of the maxillary bone after 1-week treatment of CeO_2 NPs; (b) the statistical analysis of the CEJ–ABC distance after 1-week treatment of CeO_2 NPs; (c) different views of the maxillary bone after 4-week treatment of CeO_2 NPs; and (d) the statistical analysis of the CEJ–ABC distance after 4-week treatment of CeO_2 NPs. ns means $P > 0.05$, * means $P < 0.05$, ** means $P < 0.01$, and *** means $P < 0.001$.

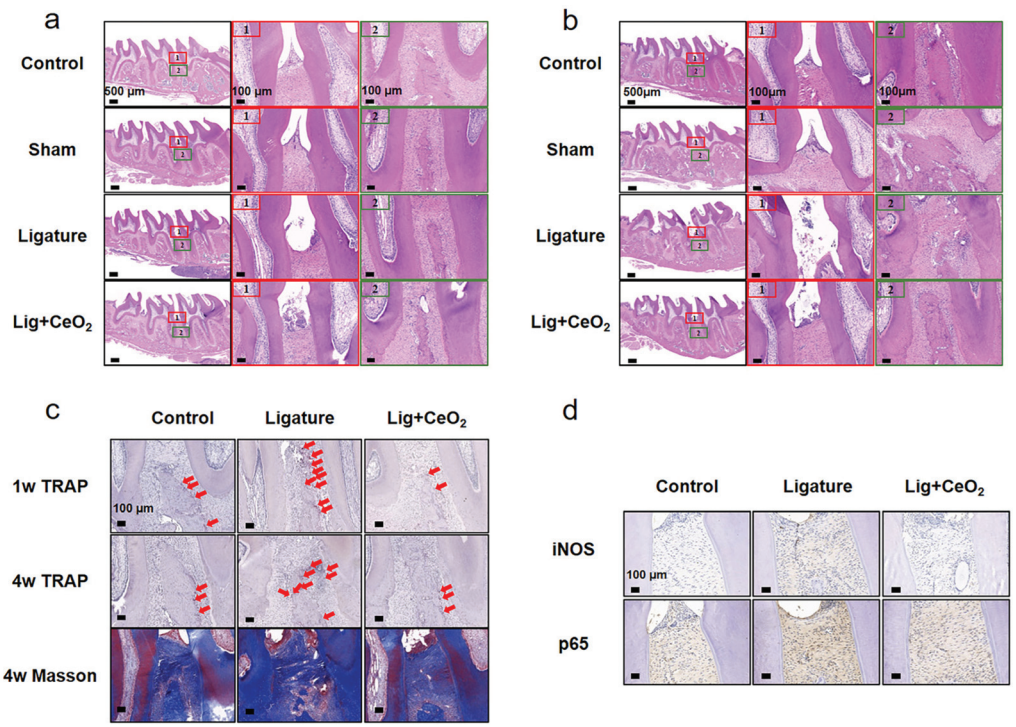

Fig. 6 The histological analysis of periodontal tissues in a rat periodontitis model. (a) HE staining of periodontal tissues around the maxillary second molar after 1-week treatment of CeO_2 NPs; (b) HE staining of periodontal tissues around the maxillary second molar after 4-week treatment of CeO_2 NPs; (c) TRAP staining and Masson's trichrome images around the maxillary second molar; and (d) immunohistochemical analysis of the inflammation of periodontal tissues around the maxillary second molar.

second molar. Maintenance of the ligature wire around the second molar in the ligature group rats additionally aggravated tissue destruction (Fig. 6b). Destruction of periodontal tissues was suppressed by injection of CeO_2 NPs in the Lig + CeO_2 group. TRAP staining revealed a decrease in the activity of osteoclasts after CeO_2 NP injection as compared to the ligature group tissues (Fig. 6b). Masson staining revealed that collagenous fibers within the periodontal ligaments were degenerated and exhibited disorderly, sparse arrangement after ligation (Fig. 6c). In the Lig + CeO_2 and control groups, however, a dense and well-organized arrangement of these fibers was noted. Evaluation of iNOS and NFκB expressions revealed marked inflammation around the maxillary second molar. Elevated iNOS and NFκB expressions in the ligature group tissues were dragged back to a little higher as compared to the control group tissues after the injection of CeO_2 NPs (Fig. 6d). The above findings thus underscored how CeO_2 NPs inhibit inflammation and attenuate tissue destruction in the setting of periodontitis. The biotoxicity of CeO_2 NPs was studied *via* evaluation of the histological sections of vital viscera (Fig. S14†). No significant differences were found among the groups.

The main point of this work was to study the potential applicability of CeO_2 NPs in the clinical management of periodontitis and elucidate their anti-inflammatory mechanism. To overcome some limitations of systemic administration, here in this study, the local injection method was adopted in keeping with other related research studies.[55,56] For example, a redox injectable gel for the treatment of periodontitis was previously reported. This gel scavenged ROS and possessed a prolonged local retention time as compared with other ROS scavengers; however, the gel was not recyclable.[57] In another study, CeO_2 contained composite nanomaterials were designed which exhibited both antibacterial and anti-inflammatory activities in the setting of photodynamic therapy.[58] The ROS-scavenging effect of CeO_2 in this study is consistent with our study.

Conclusions

In conclusion, we synthesized CeO_2 NPs exhibiting high SOD- and CAT-like activity as well as $^{\bullet}OH$ scavenging ability. These NPs exhibited ROS-scavenging activity both *in vitro* and *in vivo*. Moreover, they possessed anti-inflammatory and antioxidant activities as evidenced by the inhibition of the MAPK–NFκB signalling pathway and activation of the Nrf2–HO-1 pathway. A rat model of periodontitis revealed that CeO_2 NPs suppressed bone loss and decreased inflammation. As such, CeO_2 NPs appear to possess great promise in the clinical management of periodontitis.

Conflicts of interest

There are no conflicts to declare.

Acknowledgements

This study was supported by the Medical Science and Technology Development Foundation, Nanjing Department of Health under Grant No. YKK20153 and YKK18126, the Key Project No. ZKX19031, the National Natural Science Foundation of China under Grant No. 51772144, 51972167, 21874067, and 22104054, and the Nanjing Clinical Research Center for Oral Diseases (No. 2019060009).

References

1 O. Carcuac and T. Berglundh, *J. Dent. Res.*, 2014, **93**, 1083–1088.
2 G. Hajishengallis, *Nat. Rev. Immunol.*, 2015, **15**, 30–44.
3 A. J. Glowacki, S. Yoshizawa, S. Jhunjhunwala, A. E. Vieira, G. P. Garlet, C. Sfeir and S. R. Little, *Proc. Natl. Acad. Sci. U. S. A.*, 2013, **110**, 18525–18530.
4 F. S. C. Sczepanik, M. L. Grossi, M. Casati, M. Goldberg, M. Glogauer, N. Fine and H. C. Tenenbaum, *Periodontol. 2000*, 2020, **84**, 45–68.
5 S. Di Meo, T. T. Reed, P. Venditti and V. M. Victor, *Oxid. Med. Cell. Longevity*, 2016, **2016**, 1245049.
6 G. P. Wang, *Genome Med.*, 2015, **7**, 40.
7 C. Liu, L. Mo, Y. Niu, X. Li, X. Zhou and X. Xu, *Front. Physiol.*, 2017, **8**, 439.
8 F. Sivandzade, S. Prasad, A. Bhalerao and L. Cucullo, *Redox Biol.*, 2019, **21**, 101059.
9 M. J. Morgan and Z. G. Liu, *Cell Res.*, 2011, **21**, 103–115.
10 H. Kanzaki, S. Wada, T. Narimiya, Y. Yamaguchi, Y. Katsumata, K. Itohiya, S. Fukaya, Y. Miyamoto and Y. Nakamura, *Front. Physiol.*, 2017, **8**, 351.
11 M. Chen, W. Cai, S. Zhao, L. Shi, Y. Chen, X. Li, X. Sun, Y. Mao, B. He, Y. Hou, Y. Zhou, Q. Zhou, J. Ma and S. Huang, *J. Clin. Periodontol.*, 2019, **46**, 608–622.
12 G. Bhattarai, S. B. Poudel, S. H. Kook and J. C. Lee, *Acta Biomater.*, 2016, **29**, 398–408.
13 J. Li, Y. Li, S. Pan, L. Zhang, L. He and Y. Niu, *Biochimie*, 2019, **156**, 129–137.
14 M. A. Shaheen, S. H. Elmeadawy, F. B. Bazeed, M. M. Anees and N. M. Saleh, *Drug Delivery Transl. Res.*, 2020, **10**, 548–564.
15 C. Xu, W. Bing, F. Wang, J. Ren and X. Qu, *ACS Nano*, 2017, **11**, 7770–7780.
16 S. Jeon, S. H. Park, E. Kim, J. Y. Kim, S. W. Kim and H. Choi, *Adv. Healthcare Mater.*, 2021, e2100801, DOI: 10.1002/adhm.202100801.
17 Y. Ma, L. Chen, X. Li, A. Hu, H. Wang, H. Zhou, B. Tian and J. Dong, *Biomaterials*, 2021, **275**, 120917.
18 L. Gao, J. Zhuang, L. Nie, J. Zhang, Y. Zhang, N. Gu, T. Wang, J. Feng, D. Yang, S. Perrett and X. Yan, *Nat. Nanotechnol.*, 2007, **2**, 577–583.
19 J. Wu, X. Wang, Q. Wang, Z. Lou, S. Li, Y. Zhu, L. Qin and H. Wei, *Chem. Soc. Rev.*, 2019, **48**, 1004–1076.

20 H. Wei, L. Gao, K. Fan, J. Liu, J. He, X. Qu, S. Dong, E. Wang and X. Yan, *Nano Today*, 2021, **40**, 101269.
21 Y. Huang, J. Ren and X. Qu, *Chem. Rev.*, 2019, **119**, 4357–4412.
22 M. Liang and X. Yan, *Acc. Chem. Res.*, 2019, **52**, 2190–2200.
23 F. Natalio, R. André, A. F. Hartog, B. Stoll, K. P. Jochum, R. Wever and W. Tremel, *Nat. Nanotechnol.*, 2012, **7**, 530–535.
24 P. Zhang, D. Sun, A. Cho, S. Weon, S. Lee, J. Lee, J. W. Han, D. P. Kim and W. Choi, *Nat. Commun.*, 2019, **10**, 940.
25 X. Chen, H. Xing, Z. Zhou, Y. Hao, X. Zhang, F. Qi, J. Zhao, L. Gao and X. Wang, *J. Mater. Chem. B*, 2021, **9**, 1491–1502.
26 L. Huang, J. Chen, L. Gan, J. Wang and S. Dong, *Sci. Adv.*, 2019, **5**, eaav5490.
27 R. Dal Magro, A. Vitali, S. Fagioli, A. Casu, A. Falqui, B. Formicola, L. Taiarol, V. Cassina, C. A. Marrano, F. Mantegazza, U. Anselmi-Tamburini, P. Sommi and F. Re, *Antioxidants*, 2021, **10**, 266.
28 H. J. Kwon, M. Y. Cha, D. Kim, D. K. Kim, M. Soh, K. Shin, T. Hyeon and I. Mook-Jung, *ACS Nano*, 2016, **10**, 2860–2870.
29 N. Gao, K. Dong, A. D. Zhao, H. J. Sun, Y. Wang, J. S. Ren and X. G. Qu, *Nano Res.*, 2016, **9**, 1079–1090.
30 J. Kim, H. Y. Kim, S. Y. Song, S. H. Go, H. S. Sohn, S. Baik, M. Soh, K. Kim, D. Kim, H. C. Kim, N. Lee, B. S. Kim and T. Hyeon, *ACS Nano*, 2019, **13**, 3206–3217.
31 I. Kalashnikova, S. J. Chung, M. Nafiujjaman, M. L. Hill, M. E. Siziba, C. H. Contag and T. Kim, *Theranostics*, 2020, **10**, 11863–11880.
32 S. Zhao, Y. X. Li, Q. Y. Liu, S. R. Li, Y. Cheng, C. Q. Cheng, Z. Y. Sun, Y. Du, C. J. Butch and H. Wei, *Adv. Funct. Mater.*, 2020, **30**, 2004692.
33 J. Wu, Y. Yu, Y. Cheng, C. Cheng, Y. Zhang, B. Jiang, X. Zhao, L. Miao and H. Wei, *Angew. Chem., Int. Ed.*, 2021, **60**, 1227–1234.
34 Z. Chen, Z. Wang, J. Ren and X. Qu, *Acc. Chem. Res.*, 2018, **51**, 789–799.
35 J. Chen, S. Patil, S. Seal and J. F. McGinnis, *Nat. Nanotechnol.*, 2006, **1**, 142–150.
36 Y. Li, X. He, J.-J. Yin, Y. Ma, P. Zhang, J. Li, Y. Ding, J. Zhang, Y. Zhao, Z. Chai and Z. Zhang, *Angew. Chem., Int. Ed.*, 2015, **54**, 1832–1835.
37 Y. Zhao, Y. Wang, A. Mathur, Y. Wang, V. Maheshwari, H. Su and J. Liu, *Nanoscale*, 2019, **11**, 17841–17850.
38 D. Jiang, D. Ni, Z. T. Rosenkrans, P. Huang, X. Yan and W. Cai, *Chem. Soc. Rev.*, 2019, **48**, 3683–3704.
39 N. Singh, S. K. NaveenKumar, M. Geethika and G. Mugesh, *Angew. Chem., Int. Ed.*, 2021, **60**, 3121–3130.
40 K. Korschelt, R. Schwidetzky, F. Pfitzner, J. Strugatchi, C. Schilling, M. von der Au, K. Kirchhoff, M. Panthöfer, I. Lieberwirth, M. N. Tahir, C. Hess, B. Meermann and W. Tremel, *Nanoscale*, 2018, **10**, 13074–13082.
41 P. Lin, M. Cao, F. Xia, H. Liao, H. Sun, Q. Wang, J. Lee, Y. Zhou, Y. Guan, C. Zhang, Z. Xu, F. Li, J. F. Wei and D. Ling, *Adv. Sci.*, 2021, **8**, 2004115.
42 Z. Wang, X. Shen, X. Gao and Y. Zhao, *Nanoscale*, 2019, **11**, 13289–13299.
43 C. Xu and X. Qu, *NPG Asia Mater.*, 2014, **6**, e90.
44 S. Seal, A. Jeyaranjan, C. J. Neal, U. Kumar, T. S. Sakthivel and D. C. Sayle, *Nanoscale*, 2020, **12**, 6879–6899.
45 H. Yu, F. Jin, D. Liu, G. Shu, X. Wang, J. Qi, M. Sun, P. Yang, S. Jiang, X. Ying and Y. Du, *Theranostics*, 2020, **10**, 2342–2357.
46 S. W. Choi, B. G. Cha and J. Kim, *ACS Nano*, 2020, **14**, 2483–2496.
47 C. L. Bigarella, R. Liang and S. Ghaffari, *Development*, 2014, **141**, 4206–4218.
48 C. C. Winterbourn, *Nat. Chem. Biol.*, 2008, **4**, 278–286.
49 P. Dandona, K. Thusu, S. Cook, B. Snyder, J. Makowski, D. Armstrong and T. Nicotera, *Lancet*, 1996, **347**, 444–445.
50 P. Wang, J. Geng, J. Gao, H. Zhao, J. Li, Y. Shi, B. Yang, C. Xiao, Y. Linghu, X. Sun, X. Chen, L. Hong, F. Qin, X. Li, J. S. Yu, H. You, Z. Yuan, D. Zhou, R. L. Johnson and L. Chen, *Nat. Commun.*, 2019, **10**, 755.
51 S. K. Powers, E. E. Talbert and P. J. Adhihetty, *J. Physiol.*, 2011, **589**, 2129–2138.
52 V. Selvaraj, N. Nepal, S. Rogers, N. D. Manne, R. Arvapalli, K. M. Rice, S. Asano, E. Fankhanel, J. J. Ma, T. Shokuhfar, M. Maheshwari and E. R. Blough, *Biomaterials*, 2015, **59**, 160–171.
53 M. Mittal, M. R. Siddiqui, K. Tran, S. P. Reddy and A. B. Malik, *Antioxid. Redox Signaling*, 2014, **20**, 1126–1167.
54 X. Bao, J. Zhao, J. Sun, M. Hu and X. Yang, *ACS Nano*, 2018, **12**, 8882–8892.
55 C. Ren, X. Hao, L. Wang, Y. Hu, L. Meng, S. Zheng, F. Ren, W. Bu, H. Wang, D. Li, K. Zhang and H. Sun, *Adv. Healthcare Mater.*, 2021, **10**, e2100196.
56 C. Ni, J. Zhou, N. Kong, T. Bian, Y. Zhang, X. Huang, Y. Xiao, W. Yang and F. Yan, *Biomaterials*, 2019, **206**, 115–132.
57 M. Saita, J. Kaneko, T. Sato, S. S. Takahashi, S. Wada-Takahashi, R. Kawamata, T. Sakurai, M. C. Lee, N. Hamada, K. Kimoto and Y. Nagasaki, *Biomaterials*, 2016, **76**, 292–301.
58 Y. Sun, X. Sun, X. Li, W. Li, C. Li, Y. Zhou, L. Wang and B. Dong, *Biomaterials*, 2021, **268**, 120614.